Inorganic Chemistry

Article

pubs.acs.org/IC

Ab Initio Investigation of the UO_3 Polymorphs: Structural Properties and Thermodynamic Stability

Nicholas A. Brincat,[†] Stephen C. Parker,*[,†] Marco Molinari,[†] Geoffrey C. Allen,[‡] and Mark T. Storr[§]

[†]Department of Chemistry, University of Bath, Claverton Down, Bath, Avon, BA2 7AY, United Kingdom

[‡]Interface Analysis Centre, University of Bristol, Bristol, BS2 8BS, United Kingdom

[§]AWE, Aldermaston, Reading, Berkshire, RG7 4PR, United Kingdom

Supporting Information

ABSTRACT: Uranium trioxide (UO_3) is known to adopt a variety of crystalline and amorphous phases. Here we applied the Perdew–Burke–Ernzerhof functional + U formalism to predict structural, electronic, and elastic properties of five experimentally determined UO_3 polymorphs, in addition to their relative stability. The simulations reveal that the methodology is well-suited to describe the different polymorphs. We found better agreement with experiment for simpler phases where all bonds are similar (α- and δ-), while some differences are seen for those with more complex bonding (β-, γ-, and η-), which we address in terms of the disorder and defective nature of the experimental samples. Our calculations also predict the presence of uranyl bonds to affect the elastic and electronic properties. Phases containing uranyl bonds tend to have smaller band gaps and bulk moduli under 100 GPa contrary to those without uranyl bonds, which have larger band gaps and bulk moduli greater than 150 GPa. In line with experimental observations, we predict the most thermodynamically stable polymorph as γ-UO_3, the least stable as α-UO_3, and the most stable at high pressure as η-UO_3.

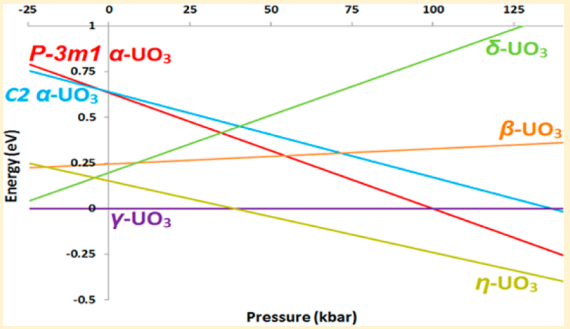

1. INTRODUCTION

The uranium oxygen system has been the subject of considerable research over the last 60 years[1−10] primarily due to the role of uranium dioxide (UO_2) in nuclear fuel cycles. Consequently most research has focused on the UO_2 phase,[11−22] and hence there is a paucity of data in the literature for the higher oxides. However, the nuclear fuel cycle commonly exposes UO_2 to oxidizing conditions, and other binary uranium oxides form at various stages (e.g., uranium is commonly mined as UO_3, and spent fuel is oxidized to U_3O_8).[23] In addition to the relatively well-characterized UO_2, the stable uranium oxides include U_4O_9, U_3O_7, U_2O_5, U_3O_8, and UO_3,[24] covering O/U ratios from 2 to 3 and containing uranium in IV, V, and VI oxidation states. The crystal structures of the uranium oxides may be broadly split into two categories, namely, the fluorite-based materials ranging from UO_2 to γ-U_2O_5, which have a more densely packed structure (around 11g cm^{-3}), and the layered-type oxides from δ-U_2O_5 to UO_3, which have more open structures, resulting in lower densities of approximately 8.5 g cm^{-3}.[4] The UO_{2+x} region for $x < 0.5$ is considered to consist of UO_2 supercells containing arrangements of oxygen defects; point interstitials for x up to approximately 0.13 and defect clusters for higher values of x.[15,19,25−27]

The focus of the present work is the oxide of uranium with the highest oxygen content, UO_3, which is most significant to the front end of the nuclear fuel cycle in the mining, milling, refinement, and conversion stages that occur prior to isotope enrichment.[28] Additionally, UO_3 can be produced from the refinement of spent nuclear fuel to be reprocessed. The UO_3 polymorph formed is characteristic of the particular production method used; thus, a detailed understanding of the UO_3 system has potential use in nuclear forensics.[29] There are seven known crystalline modifications of UO_3 (α-, β-, γ-, δ-, ε-, ζ-, and η-)[4,30] and one amorphous phase. A number of these oxides (α-, β-, γ-, and η-UO_3) are reported to feature two shorter, collinear "uranyl" type bonds akin to those observed in the UO_2^{2+} (uranyl) ion. ε- and ζ-UO_3 may also contain uranyl-type coordination; however, the atomic coordinates of these phases are yet to be resolved, leading to their exclusion from the present work. This comes despite multiple reports on the synthesis of ζ-UO_3[31,32] and ε-UO_3.[33,34] The most extensive investigation of UO_3 was into the thermodynamic properties as these hold the most significance to the reprocessing and refining processes through which UO_3 enters the fuel cycle.[35] Thermodynamic properties reported include standard free energies of formation, enthalpies of formation, entropies, and heat capacities. Sweet et al. have investigated a number of UO_3 polymorphs and their hydration products using optical spectroscopies with the aim of producing signatures for nuclear forensics applications.[29] X-ray photoelectron spectroscopy (XPS) was utilized by Bagus et al. to characterize the U(VI) oxidation state from satellite peaks, establishing that satellite

Received: April 7, 2014
Published: November 18, 2014

intensity is strongly dependent on UO distance.[36,37] Girgis et al. report values for band gaps of some of the UO_3 phases[32] but do not indicate whether they recorded these measurements themselves or obtained them from elsewhere. The values presented are significantly larger than those described in subsequent studies. They also present densities for each phase that are significantly lower than the other experimental or theoretically determined values. Idriss also published a review of uranium oxides in which band gap energies are reported for a number of UO_3 modifications.[10] Most recently He et al. have used the Cody, Tauc, and T-L methods to determine the band gap of α-UO_3,[38] with the results comparing well to those of Idriss. Using density functional theory (DFT) (local spin density approximation (LSDA) + U and HSE) He et al. also calculated the band gaps of α-, δ-, and γ-UO_3. Geng et al. also calculated the band gap of δ-UO_3, using DFT (Perdew–Burke–Ernzerhof functional (PBE)).[39] Pickard et al. also performed DFT calculations on α-, δ-, and η-UO_3, reporting lattice parameters and atomic coordinates.[40]

Previous computational work in the literature is fragmented, usually dealing only with a single or two UO_3 polymorphs. In the present work we study α-, β-, γ-, δ-, and η-UO_3 (including multiple structures for the α- and γ-polymorphs), examining the structural and elastic properties of each. This is followed by an assessment of their electronic properties and finally an evaluation of their relative thermodynamic stability. As such this work forms the most complete computational study of UO_3 to date, with consistent methodology applied throughout for simple, direct comparison of the results.

2. THEORY

2.1. DFT Methodology. The DFT calculations were all performed using the Vienna Ab Initio Simulation Package (VASP[41]) using the PBE[42] functional within the projector augmented wave method. PBE is a generalized gradient approximation functional (GGA) that builds on the LSDA by adding the gradient of the local spin density to the system energy. Consequently the GGA offers improved performance for calculating lattice parameters, electronic properties, and energies over the LSDA.

The GGA calculations described here also employ the DFT + U methodology, implemented within the simplified rotationally invariant approach introduced by Dudarev.[43] DFT + U improves the description of the strongly correlated 5f electrons, which are falsely predicted to be itinerant by the pure GGA. By incorporating an energy function that penalises noninteger f-orbital occupations the localization of f-electrons on uranium sites is realized. This is achieved in a screened HF-type manner and requires the input of the spherically averaged screened Coloumb energy (U) and the exchange energy (J), although in the Dudarev formulation only the difference between these two parameters (U_{eff}) is significant. The values of U (4.5 eV) and J (0.54 eV) used in this work were derived from the XPS experiments of Yamazaki and Kotani[44] on UO_2 and have since been used extensively for theoretical work.[45−48] We adopted these parameters for use with the UO_3 phases discussed here as no experimental values have been derived. Naturally this is an approximation as the value of these parameters will vary between compounds as the coordination, crystal structures, and uranium charges change. Previously, groups have opted to use the pure GGA for these phases without established U and J parameters.[39] The uranium electron configuration in UO_3 is $5f^0$, and so there are nominally no f electrons to be considered; however, as we demonstrate, using the GGA + U scheme improves predicted structures and band gaps over the pure GGA. Additionally it follows that the U $5f^0$ configuration means that there is no magnetic moment on the uranium atoms so competing magnetic structures and spin−orbit coupling can be safely ignored.

In each crystal structure under consideration the volume and internal structure parameters were fully relaxed with unconstrained symmetries. The electronic relaxation was performed until the total energy was converged to at least 1×10^{-6} eV/atom and the ionic relaxation was performed until the Hellmann−Feynman forces on each ion were <0.01 eV/Å. Convergence was examined on the smaller, more symmetrical, α-, δ-, and η-UO_3 systems over the 300−700 eV plane-wave cutoff energy range and $3 \times 3 \times 3$ to $9 \times 9 \times 9$ k-point grids. A cutoff energy of 500 eV was deemed sufficient to provide satisfactory convergence. An automatically generated Γ-centered Monkhorst−Pack k-point mesh was used for each calculation. The k-meshes of the larger β-and γ-UO_3 structures were selected based on the convergence data of the smaller structures. The precise number and arrangement of k-points varied between structures: α-UO_3 a $5 \times 5 \times 5$ (39 k points), β-UO_3 $4 \times 4 \times 8$ (54 k points), γ-UO_3 (128 atom cell) $6 \times 4 \times 6$ (48 k points), γ-UO_3 (64 atom cell) $6 \times 6 \times 4$ (76 k points), δ-UO_3 $12 \times 12 \times 12$ (84 k points), and η-UO_3 $6 \times 7 \times 7$ (64 k points). The k-mesh densities used fall in the range of 0.75−1.2 k-points/Å^3; well above the threshold we found was required for convergence (0.5). All figures of structures were drawn using the VESTA software.[49]

Finally, to check that the resulting structures were at a true energy minimum and there were no dynamical instabilities we calculated the phonon frequencies at the zone center in VASP using a finite displacements method. Using the PBE + U no imaginary frequencies were predicted, and so we are confident in the reliability of the structures. We also performed PBE calculations (using the same settings as the PBE + U calculations described above) and predicted a number of imaginary modes in both γ-UO_3 polymorphs. Despite our efforts to remove them we could not minimize these structures without imaginary modes. Therefore, we infer that the U parameter is essential to simulating UO_3. For comparison to the PBE + U calculations we included the PBE results in the Supporting Information, highlighting the structures that do contain imaginary modes.

2.2. Elastic Constants. The calculation of the elastic tensor is a computationally demanding process that involves calculating the response of the stress matrix on distortions of the lattice, atomic vectors, and coordinates. The elastic constants are then derived from this stress−strain relationship.[50] The bulk modulus is defined as the measure of a materials resistance to uniform compression; as such there are different formulas to calculate it for different lattice types. For a cubic lattice there are three unique elastic constants (C_{11}, C_{12}, and C_{44}), and the bulk modulus is calculated according to eq 1:

$$B = \frac{1}{3}(C_{11} + 2C_{12}) \tag{1}$$

In a hexagonal lattice there are five unique elastic constants (C_{11}, C_{12}, C_{13}, C_{33}, and C_{55}), and the bulk modulus[51] is calculated by eq 2:

$$B = \frac{2}{9}(C_{11} + C_{12} + C_{13} + C_{33}/2) \tag{2}$$

dx.doi.org/10.1021/ic500791m | Inorg. Chem. 2014, 53, 12253−12264

Table 1. Predicted Properties of the UO_3 Polymorphs

phase	method	lattice parameters (Å)			c/a ratio (Δ%)[a]	vol/U (Å^3) (Δ%)[a]	β (deg)	uranyl bond (Å)		space group[b]	energy (eV)[c]
		a (Δ%)[a]	b (Δ%)[a]	c (Δ%)[a]				U1	U2		
$P\bar{3}m1$ α-UO_3	exp[55]	3.97	3.97	4.17	1.05	56.92	120.0	2.08		$P\bar{3}m1$	
	PBE + U	3.85 (−3.1)	3.85 (−3.1)	4.18 (0.4)	1.09 (3.6)	53.64 (−5.8)	120.0	2.09		$P\bar{3}m1$	−34.34
(*)$C2mm$ α-UO_3[d]	exp[56]	3.91	6.94	4.17		56.55	90.0	2.08	2.08	$C2mm$	
	PBE + U	3.96 (1.3)	6.81 (−1.9)	4.18 (0.2)		56.31 (−0.41)	90.0	2.09	2.09	$C2mm$	−34.11
$C2$ α-UO_3[e]	exp[56]	3.91	6.94	4.17		56.55	90.0	2.08	2.08	$C2$	
	PBE + U	3.89 (−0.7))	6.61 (−4.7)	4.18 (0.4)		53.69 (−5.1)	90.0	2.09	2.09	$C2$	−34.33
β-UO_3	exp[57]	10.34	14.33	3.91		57.22	99.0			$P2_1$	
	PBE + U	10.81 (4.6)	14.33 (−0.0)	4.19 (7.2)		64.95 (13.5)	90.8			$P2_1$	−34.76
$I4_1$ γ-UO_3	exp[58]	6.90	6.90	19.98	2.89	59.46	90.0	1.80	1.89	$I4_1$	
	PBE + U	7.02 (1.8)	7.02 (1.8)	20.68 (3.4)	2.94 (1.6)	63.82 (7.1)	90.0	1.78	1.87	$I4_1$	−34.97
$Fddd$ γ-UO_3	exp[58]	9.79	19.93	9.71	2.02	59.16	90.0	1.76	1.88	$Fddd$	
	PBE + U	9.94 (1.2)	20.68 (4.2)	9.93 (3.1)	2.08 (2.9)	63.79 (8.7)	90.0	1.78	1.87	$Fddd$	−34.97
δ-UO_3	exp[59]	4.17	4.17	4.17		72.25	90.0			$Pm\bar{3}m$	
	PBE + U	4.20 (0.8)	4.20 (0.8)	4.20 (0.8)		73.89 (2.3)	90.0			$Pm\bar{3}m$	−34.78
η-UO_3	exp[30]	7.51	5.47	5.22		53.62	90.0	1.85/1.80		$P2_12_12_1$	
	PBE + U	7.76 (3.3)	5.56 (1.6)	5.34 (2.3)		57.60 (7.4)	90.0	1.84/1.82		$P2_12_12_1$	−34.82

[a]Δ% is the percentage difference between our calculated structure and experiment. [b]Space groups are calculated to a tolerance of 0.001 Å using Materials Studio.[54] [c]Reported energies are per uranium atom. [d]$C2mm\alpha$-UO_3 refers to the experimental structure (with an imaginary frequency (*)). [e]$C2$ α-UO_3 is our adjusted structure (with no imaginary frequencies).

For an orthorhombic lattice there are nine independent elastic constants (C_{11}, C_{22}, C_{33}, C_{44}, C_{55}, C_{66}, C_{12}, C_{13}, and C_{23}), and the bulk modulus is calculated according to eq 3:[52]

$$B = \frac{\Lambda}{(1 + \alpha + \beta)^2} \tag{3}$$

where Λ, α, and β are defined by eqs 4, 5, and 6, respectively:

$$\Lambda = C_{11} + 2C_{12}\alpha + C_{22}\alpha^2 + 2C_{13}\beta + C_{33}\beta^2 + 2C_{23}\alpha\beta \tag{4}$$

$$\alpha = \frac{(C_{11} - C_{12})(C_{33} - C_{13}) - (C_{23} - C_{13})(C_{11} - C_{13})}{(C_{33} - C_{13})(C_{22} - C_{12}) - (C_{13} - C_{23})(C_{12} - C_{23})} \tag{5}$$

$$\beta = \frac{(C_{22} - C_{12})(C_{11} - C_{13}) - (C_{11} - C_{12})(C_{23} - C_{12})}{(C_{22} - C_{12})(C_{33} - C_{13}) - (C_{12} - C_{23})(C_{13} - C_{23})} \tag{6}$$

The bulk modulus for monoclinic and triclinic cells, with 13 and 21 unique elastic constants, respectively, were obtained by averaging the first nine elastic constants (C_{11}–C_{33}), a method that provides equivalent results to the formulas described above.

The bulk modulus can also be calculated by performing an expansion (and contraction) of the unit cell and computing the energy at each point. These data can then be fitted to the second or third order Birch–Murnaghan equation of state[53] to yield the bulk modulus. We tested these methods for hexagonal $P\bar{3}m1$ α-UO_3 and cubic $Pm3m$ δ-UO_3, finding agreement with our chosen method to within 3%.

3. RESULTS AND DISCUSSION

We first discuss the predicted structural properties of the UO_3 polymorphs along with a comprehensive comparison of the available previous experimental and computational data (Section 3.1). We then present the simulated neutron diffraction patterns (Section 3.2), elastic properties (Section 3.3), and electronic properties (Section 3.4). We conclude with an assessment of the relative UO_3 stabilities (Section 3.5).

3.1. Crystal Structures. Table 1 lists the predicted structural data of each polymorph (complete crystallographic data is in the Supporting Information). Validity of our predicted structures was assessed by calculating the vibrational frequencies and confirming the absence of imaginary modes.

3.1.1. α-UO_3. α-UO_3 is structurally related to α-U_3O_8 with uranium deficiencies and is typically prepared by heating of uranyl peroxide to 400–500 °C.[60] The structure was initially identified to crystallize in a four-atom hexagonal unit cell with the $P\bar{3}m1$ space group by Zachariasen using X-ray diffraction (XRD)[55] but was later refined by Loopstra et al.[56] and Greaves et al.[61] to orthorhombic $C2mm$ and $C222$, respectively, both featuring two formula units per cell. Discrepancies between the experimentally determined densities by Zachariasen and Loopstra et al., 7.04 and 7.25 g cm^{-3}, respectively, and the calculated one from Loopstra et al. (8.39 g cm^{-3}) are significant, leading Greaves et al. to conclude that α-UO_3 is an imperfect orthorhombic structure with approximately 12% of uranium lattice sites vacant, reducing the theoretical density to 7.44 g cm^{-3}, which is closer to experimental observations. Consequently the structure they obtained is complex and involves partial occupancy of the uranium and oxygen sites; information is missing from the available structural data, and so hindering our simulation efforts. Thus, only the original hexagonal $P\bar{3}m1$ modification (Figure 1a) and orthorhombic $C2mm$ structure (Figure 1b), which both produce stoichiometric unit cells, were considered in the present study. Both structures have two distinct oxygen sites; O1 is the axial oxygen contributing to the uranyl-type group, and O2 is found lying in the equatorial (110) plane. A slight distortion of the O2 atoms above and below this plane results in distorted hexagonal bipyramdial coordination.

Table 1 contains the predicted structural properties of $P\bar{3}m1$ and $C2mm$ α-UO_3 as well as the calculated energy per uranium ion, and Figure 1c,d and Figure 2a,c displays their calculated structures. Overall structural reproduction of the $P\bar{3}m1$

dx.doi.org/10.1021/ic500791m | Inorg. Chem. 2014, 53, 12253–12264

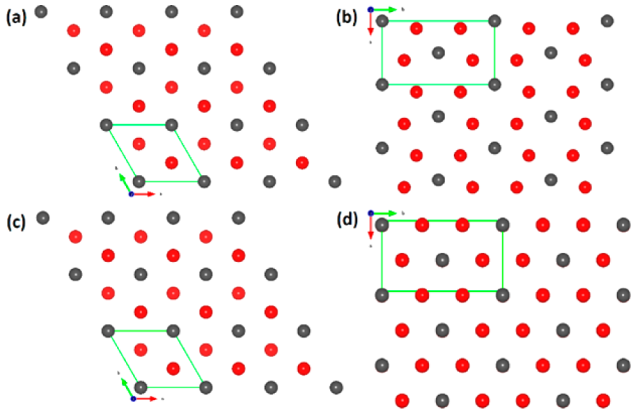

Figure 1. Structures of α-UO_3 polymorphs; the unit cell is highlighted in green, uranium ions are black and oxygen are red (a) experimentally observed $P\bar{3}m1$ structure, (b) experimentally observed $C2mm$ structure, (c) PBE + U $P\bar{3}m1$ structure, and (d) PBE + U $C2mm$ ($Amm2$) structure.

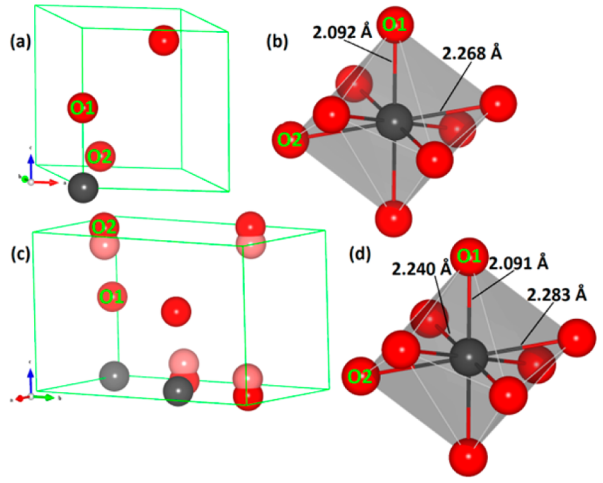

Figure 2. PBE + U predicted structures of α-UO_3 polymorphs: (a) $P\bar{3}m1$ hexagonal unit cell, (b) uranium coordination in $P\bar{3}m1$ α-UO_3, (c) $C2mm$/$C2$ orthorhombic unit cell, and (d) uranium coordination in $C2$ α-UO_3. In (c) pink spheres represent the adjusted ($C2$) equatorial oxygen positions.

polymorph is very good, maintaining the same space group and coordination as reported experimentally. However, contrary to expectations the unit cell volume is slightly underestimated (PBE + U normally overestimates lattice parameters). For the $P\bar{3}m1$ modification the PBE + U predicted volume of 53.64 $Å^3$/U matches well with the LSDA + U result of He et al.[38] (53.91 $Å^3$/U), while Pickard et al. report a larger underestimation of 51.83 $Å^3$/U using the Local Density Approximation (LDA).[40] The c/a ratio in $P\bar{3}m1$ is overestimated by 3.6%, arising from the slight underestimation of the a lattice parameter.

The experimentally derived $C2mm$ orthorhombic structure was also well-reproduced by our calculations, albeit with a distortion to more isotropic coordination (Figure 1b,d), closer in line to the $P\bar{3}m1$ structure (Figure 1a,c). However, the $C2mm$ structure gave a single imaginary frequency, which was removed by displacing the equatorial oxygen atoms along the c axis above and below the (110) plane (Figure 2c), resulting in a reduced-symmetry $C2$ structure. This new arrangement bears greater resemblance to the $P\bar{3}m1$ structure, which also features equatorial oxygen ions shifted above and below the plane in puckered hexagonal bipyramidal coordination. On relaxation the similarity of the $C2$ polymorph with the $P\bar{3}m1$ becomes even more striking with a very small energetic preference for $P\bar{3}m1$ (0.01 eV/U) and a difference in predicted volumes of less than 0.05 $Å^3$/U (Table 1). By comparison the $C2mm$ polymorph was predicted to be 0.22 eV/U less stable than either of the other structures. Six oxygen ions coordinating in the same equatorial plane clearly destabilizes the structure. Lifting this structural frustration by shifting the oxygen out of the plane removes the imaginary vibrational mode, with a significant stabilization effect (see energies in Table 1).

The predicted axial bond length is 2.09 Å in both structures (compared to an observed 2.08 Å). Although shorter than the other U−O bonds present this is too long for the bonds to be considered "uranyl"-type. The equatorial bonds are 2.27 Å ($P\bar{3}m1$) and 2.24 and 2.28 Å ($C2$) (2.40, 2.02, and 2.16 Å in experiment, respectively) (Figure 2b,d). This represents a loss of anisotropy in the $C2$ polymorph, further shifting the structure toward that of the $P3m1$ modification. Additionally the space groups for the hexagonal ($P\bar{3}m1$) and orthorhombic ($C2$) polymorphs are in a group−subgroup relation and so are linked by symmetry. Considering this preference for more isotropic bonding as well as "puckered" equatorial coordination over planar it is logical that the $C2mm$ polymorph is a thermally averaged structure. In α-UO_3 the equatorially coordinated oxygen ions exist above and below the plane but have enough thermal energy to shift their relative positions such that the equilibrium site lies precisely in the (100) plane (i.e., red spheres in Figure 2c). This fully explains our lower calculated stability and the imaginary vibrational frequency for $C2mm$ α-UO_3.

3.1.2. β-UO_3. β-UO_3 is produced by calcining the product of the reaction of uranyl nitrate and ammonia at 450−500 °C; at lower temperature γ-UO_3 forms so heating must be rapid. β-UO_3 was determined to have a monoclinic unit cell with the $P2_1$ space group (Figure 3a−c) using XRD and neutron diffraction.[57,62] The structure contains five unique U and 15 O sites in a semilayered structure: U1−3 are found on the (010) plane and are connected by O1−5 to form a single UO layer; U4 and U5 are situated midway between these layers, interconnected by O12−15; the remaining O6−11 bridge the two types of layers. The coordination of uranium at each site, as reported in the original experimental publication, is either distorted octahedral (U3, U4, and U5) or irregular 7-fold (U1 and U2), with each featuring a single short U−O bond (1.51−1.79 Å) and five or six U−O bonds at least 0.5 Å longer. However, analyzing the experimentally derived structure with bond cut-offs set according to the reported shortest and longest bonds it is revealed that there is only a single distorted octahedral site (U3) with the other uranium ions in irregular 7-fold coordination (Figure 3a). The distorted coordination averts the formation of the full uranyl group in each case, even if there are two shorter bonds (e.g., U4). There is good agreement between the observed and calculated densities for this polymorph; 8.25 and 8.30 g cm^{-3}, respectively.[63] There are no pre-existing computational studies of β-UO_3 in the literature, so this investigation forms the first theoretical treatment of the phase.

The calculated structural properties of β-UO_3 can be found along with the experimental data in Table 1. Figure 3d−f displays the calculated β-UO_3 structure. The lattice parameters and unit cell volume are overestimated; giving a total 13.5% volume increase. The reproduction of individual lattice

dx.doi.org/10.1021/ic500791m | *Inorg. Chem.* 2014, 53, 12253−12264

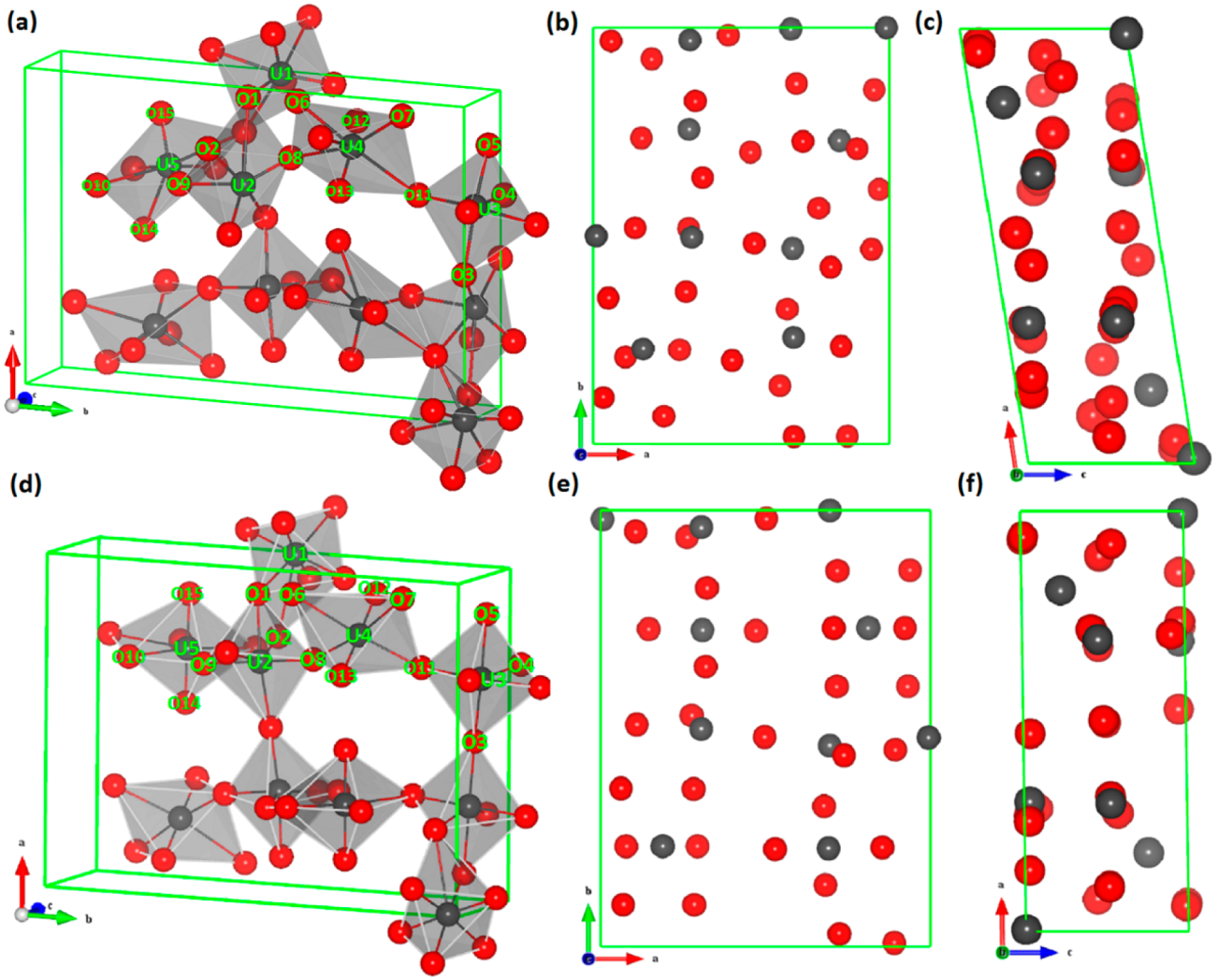

Figure 3. β-UO_3 unit cell: (a–c) observed experimental structure and (d–f) PBE + U calculated structure. (a) and (d) show the coordination at the uranium sites, (b) and (e) show the projection along the z axis, and (c) and (f) show the projection along the y axis.

parameters is considerably better, with 4.6, 0.0, and 7.2% overestimations of a, b, and c, respectively. The monoclinic symmetry and $P2_1$ space group are retained on minimization, although there is noticeable change in the bond lengths and uranium coordination at U2 and U4 sites (Figure 3). The bond lengths of the relaxed structure are more consistent with the expected U–O bond lengths for uranium oxides than the experimental ones with none shorter than 1.76 Å (compared to 1.51 Å experimentally). There is also the emergence of collinear, uranyl-type bonding at U1, U4, and U5 sites with bonds ranging from 1.76 to 1.81 Å. There is only a slight increase in average bond length (0.9%); this reflects a decrease in anisotropy (similar to that in $C2$ α-UO_3) as there is a clear preference for more homogeneous UO bonding. The isotropic shift is also demonstrated by the uranium coordination change at U2 and U4, where the loosely coordinated oxygen is lost in each case to give distorted octahedral coordination.

Given the emergence of uranyl-type bonds, more regular uranium coordination environments, and the loss of the unphysically short bonds leads us to suggest that a large amount of disorder is present in the experimental β-UO_3 structure.

3.1.3. γ-UO_3. γ-UO_3 is acknowledged as the thermodynamically stable polymorph at oxygen pressures <10 atm.[64] It is prepared by burning uranyl nitrate hexahydrate in air at 400–600 °C or heating other UO_3 modifications to 650 °C in 40 atm O_2.[3] Using XRD Engmann et al. first determined the structure, describing it as tetragonal with space group $I4_1$, although with γ = 90.34° it is formally monoclinic.[65] Loopstra et al. later performed neutron diffraction experiments on γ-UO_3 over a range of temperatures, identifying it to be orthorhombic $Fddd$ at ≤293 K (Figure 4a,b) but forming a tetragonal $I4_1$ phase >373 K (Figure 5a,b), the former space group being a maximal subgroup of the latter.[58] The orthorhombic cell has twice the number of atoms and is double the volume of the tetragonal cell. The two cells contain two types of uranium site; one in distorted octahedral coordination (U1); the other in distorted dodecahedral coordination (U2) and three unique oxygen locations. O1 sites form short equatorial bonds with U2 atoms and coordinate in a uranyl manner with U1 sites; O2 atoms are equatorially coordinated to U1 atoms and form the other type of short equatorial bond with U2; O3 form the longer equatorial bonds with U2, as well as providing their uranyl-type coordination. The monoclinic Engmann structure also shares the bonding and coordination environments of the Loopstra et al. structures. Calculated densities for the $Fddd$ and $I4_1$ structures are in good agreement (8.00 ± 0.02g cm^{-3}) and compare favorably with the experimentally determined value for

dx.doi.org/10.1021/ic500791m | *Inorg. Chem.* 2014, 53, 12253–12264

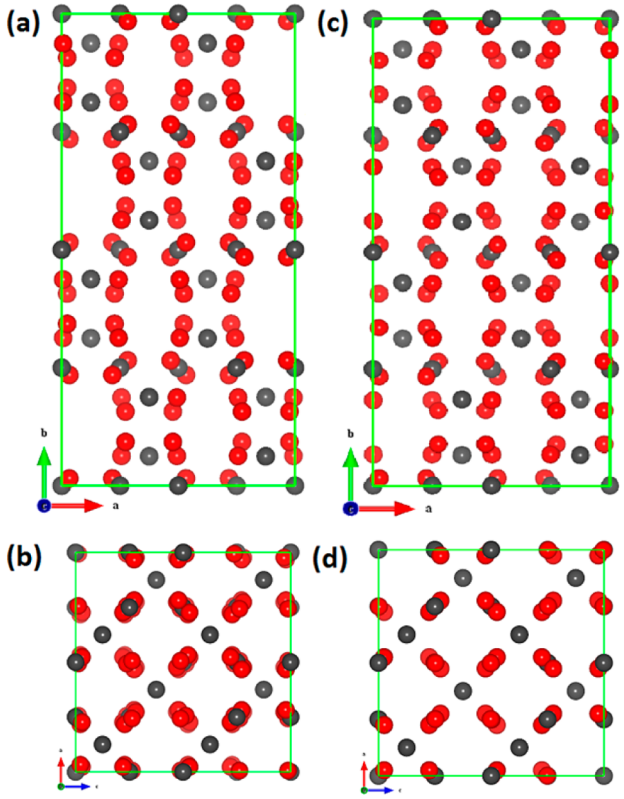

Figure 4. *Fddd* γ-UO_3 unit cell: (a) and (b) experimental, (c) and (d) PBE + U calculated.

the Engmann structure (8.02g cm^{-3}).[65] The $I4_1$ polymorph was modeled using LDA + U by He et al.[38] and shows reasonable agreement with the observed volume (−3%), although no other structural information is provided.

The monoclinic structure was found to relax to a tetragonal cell, retaining the $I4_1$ symmetry, with the same predicted energy and bond lengths as the $I4_1$ structure reported by Loopstra et al.[58] This leads us to conclude that the observed monoclinic modification is most likely the same structure as that observed by Loopstra; indeed, the reported deviation of β from 90° is very small (0.34°). The predicted structural data for $I4_1$ and *Fddd* γ-UO_3 are in Table 1, while Figure 4c,d shows the calculated *Fddd* structure and Figure 5c,d shows the $I4_1$; demonstrating the good overall agreement with experiment.

The minimized $I4_1$ and *Fddd* structures are extremely similar; the predicted volumes and energies per uranium are essentially identical, and the relaxed bonds are almost the same length. Indeed, the *Fddd* structure represents a 45° rotation and $\sqrt{2}$ expansion of the $I4_1$ polymorph in the x and y directions, accompanied by a reduction in symmetry in going from a tetragonal to orthorhombic cell. As the only experimental difference was the temperature the two structures were recorded at it follows that DFT does not distinguish between them well at 0 K. No significant changes are observed in our relaxed structures; the symmetry and uranium coordination was retained in both.

The lattice parameters and volume (7.1% for $I4_1$ and 8.7% for *Fddd*) were overestimated, compared to the underestimation of the LDA + U calculations of He et al.[38] (3.0%). In our calculations, this volume expansion corresponds to overestimation of each lattice parameter by <3.5% and <4.5% for the $I4_1$ and *Fddd* structures, respectively. The c/a ratio was also slightly overestimated in our calculations (1.6/2.9% for $I4_1$/*Fddd*); however, this value was not reported by He et al. The equatorially coordinated U−O bonds are predicted to lengthen slightly, more so at U2 sites than U1, with the largest increase associated with the U2−O3 equatorial bonds. These are already the longest observed bonds (3.04 and 3.01 Å for $I4_1$ and *Fddd*), and so the increase to 3.23 Å signifies very weak coordination. The uranyl-type bond lengths are predicted to decrease slightly to 1.87 Å. γ-UO_3 is the first UO_3 polymorph for which there is an increase in bond anisotropy, particularly at U2 sites. This change is more or less the same for both

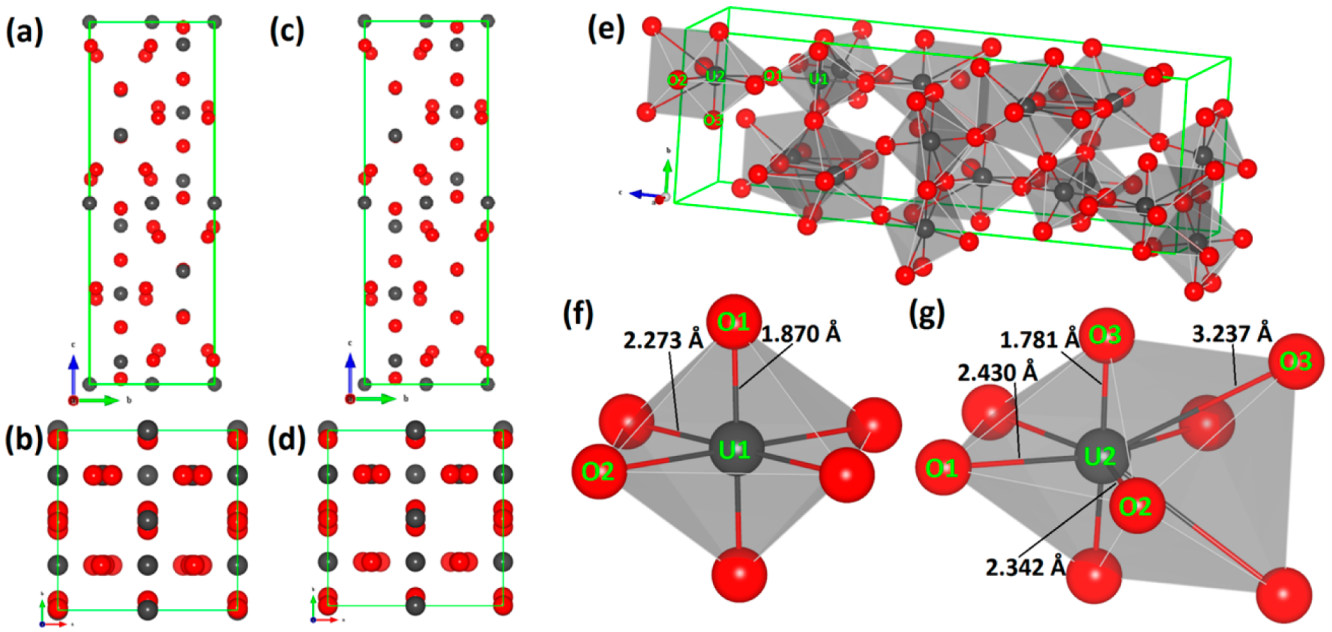

Figure 5. $I4_1$ γ-UO_3 unit cell: (a) and (b) experimental, (c) and (d) PBE + U calculated, and (e) PBE + U calculated showing coordination. (f) Octahedral uranium coordination at U1 and (g) dodecahedral uranium coordination at U2.

dx.doi.org/10.1021/ic500791m | *Inorg. Chem.* 2014, 53, 12253−12264

polymorphs given the strong resemblance between the relaxed structures. Overall these calculations point toward two very similar structures, with negligible difference in energy for conversion to occur over the experimentally specified temperature range. This thermal lability between the two structures implies the presence of disorder. This also explains the overestimation of lattice parameters and consequently the deviation of the simulations from the experimental c/a ratio, as the disorder is absent from our calculations.

3.1.4. δ-UO$_3$. δ-UO_3 is synthesized by hydrothermally reacting γ-UO_3, yielding β-$UO_2(OH)_2$, and then heating to 375 °C. This polymorph crystallizes in the $Pm\bar{3}m$ space group with the ReO_3 structure[59] (Figure 6a,b) and has theoretically

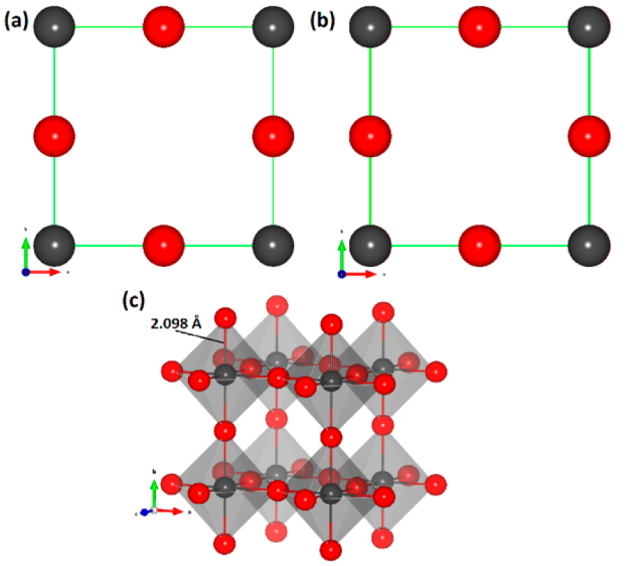

Figure 6. Structure of $Pm\bar{3}m$ δ-UO_3: (a) experimental unit cell, (b) PBE + U calculated unit cell, and (c) uranium coordination.

and experimentally determined densities of 6.99 and 6.57 g cm^{-3}, respectively.[4] δ-UO_3 contains single U and O sites with perfect octahedral coordination at the uranium atoms, signifying a lack of uranyl-type bonding. This comparatively simple composition has meant δ-UO_3 is the most-modeled UO_3 modification.[38−40]

The predicted structural properties for δ-UO_3 are in Table 1, and Figure 6b,c shows the PBE + U predicted structure. The unit cell was well reproduced, with a small change in volume (2.3%) and bond length increase (0.8%) predicted. The symmetry and coordination remained identical. Our PBE + U calculation overestimates the lattice parameters compared to the underestimation of He et al.'s HSE and LDA + U calculations[38] and Pickard et al.'s LDA calculations.[40] The PBE calculation of Geng et al.[39] agrees well with our own PBE calculation (Supporting Information).

3.1.5. η-UO$_3$. Siegel et al. used XRD to derive the lattice parameters of η-UO_3, finding it to have an orthorhombic $P2_12_12_1$ structure[30] (Figure 7a,b). The unit cell contains four formula units and a single type of uranium atom in 7-fold (puckered pentagonal bipyramidal) coordination. It features collinear uranyl-type bonds although the distortion of the polyhedra produces a slight disparity in the bond lengths (1.84 and 1.85 Å experimentally). The O1 sites only feature in collinear bonds with uranium atoms (the longer of the two). O2 atoms form the shorter collinear bond as well as one of the

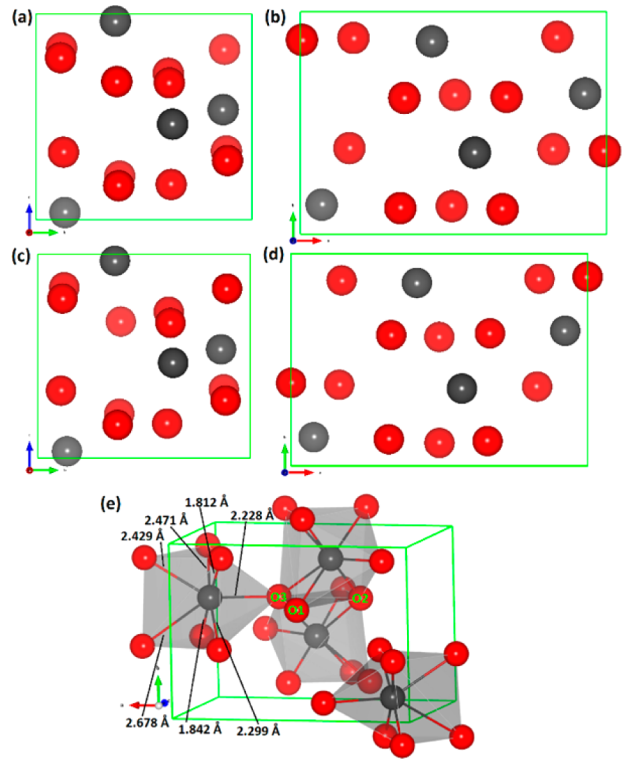

Figure 7. Structure of $P2_12_12_1$ η-UO_3: (a) and (b) experimental unit cell, (c) and (d) PBE + U calculated unit cell and (e) uranium coordination.

equatorial sites. The O3 sites only participate in equatorial uranium coordination through two undistorted locations and one significantly distorted from the regular coordination site. The precise synthesis of η-UO_3 has not been described; however, it was reportedly produced at a temperature of 1100 °C and pressure of 30 kilobars.[30] In keeping with this reputation as the high-pressure modification at 8.86 g cm^{-3} (theoretical and measured) η-UO_3 has the highest density of any UO_3 polymorph, or any layered uranium oxide for that matter.[4]

Table 1 contains the predicted structural information for η-UO_3, and Figure 7c−e shows the PBE + U predicted structure, demonstrating the good overall agreement with experiment. The lattice parameters and volume are slightly overestimated, but the symmetry and space group are well-retained. Pickard et al.[40] predict lattice parameters and volume slightly closer to the experimental values than our PBE + U calculation but offer little other structural insight. Although there is a volume expansion of 7.4% the individual lattice parameters are all reproduced to within 3.5%. Predicted uranyl bond lengths are closest to experiment at <1% difference, compared to a mean difference of 3.2% for equatorial bonds. The uranyl bonds are slightly more symmetrical than in the experimental structure, although still not entirely collinear, at 1.82 and 1.84 Å. Overall though the bonding comparison is mostly similar to γ-UO_3; a tiny increase in anisotropy is observed on relaxation when the equatorial oxygen is also accounted for. As with β- and γ-UO_3 the more irregular coordination, slightly larger discrepancy between calculated and reported lattice parameters and shift toward more collinear uranyl bonding on relaxation indicates the presence of disorder in this polymorph.

dx.doi.org/10.1021/ic500791m | Inorg. Chem. 2014, 53, 12253−12264

3.2. Simulated Neutron Diffraction Patterns. As described in the previous section, we simulated all known UO_3 polymorphs and showed that the structures are well-reproduced; particularly α- and δ-UO_3, while β-, γ-, and η-UO_3 are well-reproduced to a lesser extent. We consider that the methodology correctly captures the nature of the U^{6+}−O^{2-} system and that structural discrepancies are caused by intrinsic disorder and defects. The evidence comes from good reproduction of the wider variety of U−O bond distances and coordination found in β-, γ-, and η-UO_3. These phases contain short-range uranyl-type bonds, midrange bonds (as observed in α- and δ-UO_3), and weaker long-range bonds (in excess of 3 Å in γ-UO_3). UO_3 phases are usually defined as layered materials, and as such the inclusion of dispersion forces would be expected to impact on their structural representation. We have tested the DFT-D3 method of Grimme[66] on γ-UO_3 (the only phase to contain short, medium, and long-range bonds) and noted no real improvement. For example in $I4_1$ γ-UO_3 the DFT-D3 lattice parameters are $a = b = 6.99$ Å, $c = 20.68$ Å, $\alpha = \beta = \gamma = 90°$ (compared to $a = b = 7.02$ Å, $c = 20.68$ Å, $\alpha = \beta = \gamma = 90°$ with PBE + U). The inclusion of van der Waals interactions is important in discretely layered materials such as phases of TiS_2[67] and V_2O_5[68] where the layers are held together by dispersion forces. In the same way they would be important in similarly layered uranium minerals such as studtite or schoepite. However, in all UO_3 phases the layers are linked by bridging O atoms, and therefore the inclusion of vdW does not improve the model compared to DFT + U. This reinforces the idea that nonstoichiometry and defect chemistry are responsible for the discrepancy in lattice parameters reproduced by our stoichiometric structures. A suggestion that is well-documented as Greaves et al.[61] reported non-stoichiometry in α-UO_3, Hoekstra et al. report a $UO_{2.9}$ phase,[3] while Cornman describes the O/U ratios of their prepared UO_3 samples as ranging from 3.03 to 3.07, with ζ-UO_3 even higher at 3.27.[31] Synthesis of pure phases is also challenging; Weller et al. report that their synthesis of δ-UO_3 also produced α-UO_3,[59] and Sweet et al. describe producing 82% β-UO_3 with 18% α-UO_3.[29] Additionally as U^{6+} is soluble, hydrolysis and hydration products are known to form readily under ambient conditions.[29,69] In this section we will show further evidence of the generally good comparison between the simulated phases and experiment by means of simulated neutron diffraction patterns.

A number of the UO_3 structures were derived using neutron diffraction; however, the varying complexity of the patterns makes comparison difficult. Thus, we chose to calculate neutron diffraction patterns for each polymorph from the experimental and PBE + U predicted structures to provide a better means of comparison. The neutron diffraction patterns provide a useful visual aid for assessing the similarity between complex materials when it is difficult to directly visualize the structures. Patterns for $P\bar{3}m1$ α-, $I4_1$ γ-, and δ-UO_3 are shown in Figure 8, and the remainder can be found in the Supporting Information. All neutron diffraction patterns were calculated using the Powder Cell code.[70]

The principle observation is that the number of peaks, and their relative intensities, are found to be the same, or similar, for most of the simulated experimental and predicted structures. The main difference arises in the angle (2θ), where theory can be shifted from experiment. This arises from the difference in lattice parameters (and bond lengths) and scales with the agreement of our calculations with experiment.

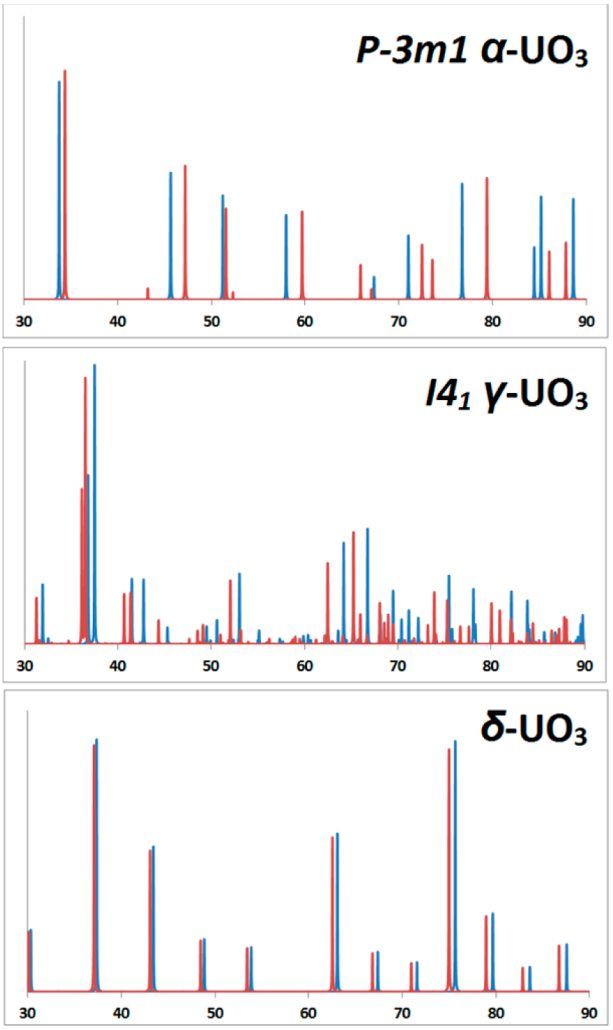

Figure 8. Calculated neutron diffraction patterns for selected UO_3 polymorphs (see the Supporting Information for the complete set). Intensity (y axis) is in arbitrary units and so has not been labeled; angle 2θ (x axis) is in degrees (deg). Blue shows the calculated pattern from the experimentally determined structure, red shows the calculated pattern for the PBE + U predicted structure.

Accordingly we see the smallest shift between the simulated experimental and PBE + U patterns in the structures with closest agreement between experimental and predicted lattice parameters. The lowest shift (slightly lower 2θ) is observed for δ-UO_3 (Figure 8), which also has the best agreement between our simulated spectra and the peaks reported in the original work;[59] this is indicative of a highly ordered structure. $P\bar{3}m1$ α-UO_3 also shows good agreement between experimental and predicted simulated spectra, although the predicted peaks are shifted to higher 2θ, reflecting the underestimation of the α-UO_3 lattice parameters. In the same way β-, $Fddd/I4_1$ γ-, and η-UO_3 have more shifted patterns and show the largest deviation from the experimentally recorded neutron diffraction patterns.[57,58] This disparity between the recorded experimental neutron diffraction patterns and our simulated patterns from the experimentally derived structures is a strong indication that these three oxides (the only three to contain uranyl bonding) are inherently more disordered and defective than the UO_3 polymorphs without uranyl bonds.

The neutron diffraction patterns are also useful for highlighting the similarities of different competing structures.

dx.doi.org/10.1021/ic500791m | Inorg. Chem. 2014, 53, 12253−12264

Table 2. PBE + U Predicted Elastic Constants and Bulk Moduli for the UO_3 Polymorphs

	elastic constants[a] (GPa)									
phase	C_{11}	C_{12}	C_{13}	C_{22}	C_{23}	C_{33}	C_{44}	C_{55}	C_{66}	bulk modulus (GPa)
$P\bar{3}m1$ α-UO_3	246.5	179.8	41.5			519.8		50.7		170.9
$C2$ α-UO_3	222.1	182.8	37.6	253.0	43.9	521.1	37.0	50.5	49.9	164.5
β-UO_3	115.6	22.2	43.9	142.8	45.0	167.1	16.7	45.9	−7.4	72.0
$I4_1$ γ-UO_3	162.1	63.4	39.5	162.2	39.5	107.4	28.9	39.1	38.9	74.8
$Fddd$ γ-UO_3	142.8	39.5	82.6	107.1	40.3	143.7	38.8	38.9	49.2	74.9
δ-UO_3	387.6	33.2					27.3			151.3
η-UO_3	172.7	55.2	60.7	120.8	70.3	150.8	29.1	63.7	46.5	89.2

[a]Independent constants for cubic (3), hexagonal (5), and orthorhombic (9) cells are included, but those for monoclinic (13) and triclinic (21) cells are not. Details of B calculation are in Section 2.2.

Looking at the two γ-UO_3 polymorphs it is clear that they are crystallographically extremely similar. They have almost identical distributions of peaks; the main difference is in their relative intensities. This is indicative of the different symmetries of the two structures as the Miller planes will be aligned differently, affecting the intensity of the detected signal. There is also a strong match between the patterns for the different α-UO_3 structures, although as there are more structural differences the patterns do not match as well as those of the different γ-UO_3 polymorphs.

3.3. Elastic Properties. There is no experimental or computational data in the literature regarding the elastic constants of UO_3, and so the results presented here form the first predicted values. Elastic constants were calculated with the PBE + U (Table 2) for the full set of polymorphs. Elastic constants for all polymorphs except γ-UO_3 (as these structures contained imaginary frequencies) calculated using the PBE can be found in the Supporting Information.

The predicted bulk moduli for the UO_3 polymorphs range from ∼75 to 171 GPa, with the precise value depending on the structure of the phase. This range is lower than the denser UO_2 (ρ = 10.97 g cm^{-3}, B = 209 GPa[12]) as would be expected for more openly structured materials. The highest bulk moduli belong to α- and δ-UO_3 (171 and 151 GPa, respectively), which, intriguingly, are the two lowest-density polymorphs examined here (7.04 and 6.57 g cm^{-3}, respectively). Considering this with the bulk moduli of β-, γ-, and η-UO_3 (72, 75, and 89 GPa, respectively) and their respective densities (8.25, 8.00, and 8.86 g cm^{-3}) there appears to be an inverse relationship between the bulk modulus and density of a UO_3 polymorph. However, the most important structural distinction between these two sets of materials is the presence or absence of uranyl bonds. Our results strongly suggest that the presence of uranyl bonding in a UO_3 polymorph (and possibly other phases) can be predicted from a determination of the bulk modulus. If it is less than 100 GPa then the oxide is likely to contain uranyl bonds (β-, γ-, and η-UO_3); if it is 150 or higher than they are probably absent (α- and δ-UO_3).

3.4. Electronic Properties. The U^{6+} ion has unoccupied 5f states ($5f^0$), this is confirmed by our results which predict each UO_3 polymorph to be a charge-transfer insulator with a valence band (VB) composed predominantly of oxygen 2p states and conductance band (CB) comprised mainly of uranium 5f states. Almost no contribution to the conductance band and small contributions to the bottom of the valence band from *6d* orbitals were observed for all polymorphs and so these have also been included in the partial density of states (PDOS), displayed in Figure 9 (The PBE calculated DOS can be found in the Supporting Information). Contributions from uranium 5f

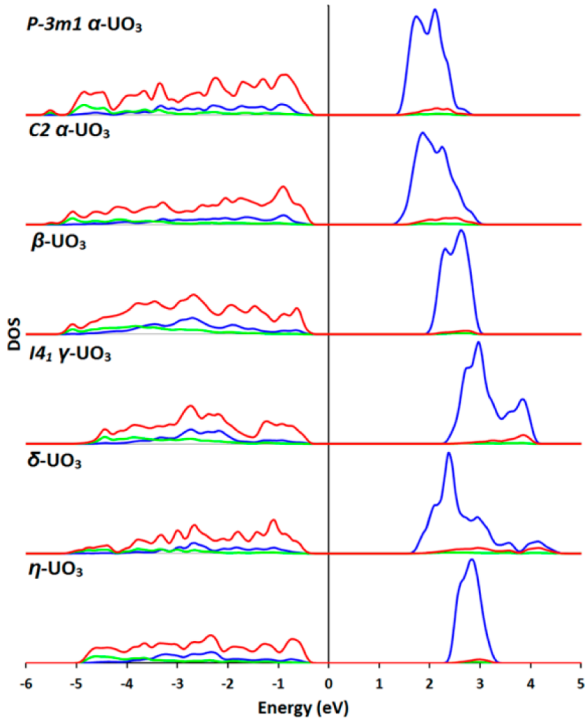

Figure 9. PBE + U calculated PDOS for the UO_3 polymorphs. Oxygen 2p states are in red, Uranium 5f states are in blue and Uranium 6d states are in green. Contributions from other states are negligible and so are omitted from the diagram. Only spin up states are included here as the spin up and spin down channels are identical. The energy of the highest occupied state in each case was set to zero eV.

orbitals are observed in the VB and from oxygen 2p in the CB, which may be attributed to hybridization - the degree of covalency in the U−O bonds. This accords well with the results of Bagus et al., who report that a closed shell system (i.e., U^{6+}) screens the 6d orbitals more effectively than a partially occupied shell (i.e., U^{4+} and U^{5+}). So we would expect to see greater contribution from the 6d orbitals in the DOS of U_3O_8 (U^{5+}/U^{6+}) and an even greater effect in UO_2 (U^{4+}) but not in UO_3.

The calculated band gaps are listed in Table 3 and data from the literature is provided where available. The GGA is renowned for generally underestimating band gaps, however it performs well here for β-, γ-, and δ-UO_3. The predicted α-UO_3 band gap is a considerable underestimate of experiment in all three of our structures. The band gap in the *C2mm* polymorph (the structure containing imaginary frequencies) is an even more significant underestimate (approximately 20%). This augments the argument that the equatorial O ions are

dx.doi.org/10.1021/ic500791m | *Inorg. Chem.* 2014, 53, 12253−12264

Table 3. Calculated and Experimental Band Gaps of UO_3 Phases Containing Uranyl-Type Groups from the Present Work and the Literature

study	phase	method	band gap (eV)
He et al.[38]	α-UO_3	experiment	2.63
He et al.[38]	$P\bar{3}m1$ α-UO_3	LDA + U	0.94
		HSE	3.10
present work		PBE + U	1.59
	$C2mm$ α-UO_3	PBE + U	0.64
	$C2$ α-UO_3	PBE + U	1.54
Idriss et al.[10]	β-UO_3	experiment	2.17
present work		PBE + U	2.11
He et al.[38]	γ-UO_3	experiment	2.38
		LDA + U	2.35
present work	$I4_1$ γ-UO_3	PBE + U	2.40
	$Fddd$ γ-UO_3	PBE + U	2.39
Idriss et al.[10]	δ-UO_3	experiment	2.17
He et al.[38]		LDA + U	2.19
		HSE	3.21
Geng et al.[39]		PBE	1.60
present work		PBE + U	2.19
present work	η-UO_3	PBE + U	2.67

displaced in $C2mm$ α-UO_3. The experimentally determined band gaps of the polymorphs that do not contain uranyl-type bonds in our calculations (α- and δ-UO_3, 1.59 and 2.19 eV respectively) seem to be lower than those that do (γ- and η-UO_3, 2.40 and 2.67 eV respectively). However, β-UO_3 (for which we predict uranyl bonds at three out of five sites) has a relatively low band gap of 2.11 eV and so this trend is weaker than the uranyl-bulk modulus relationship noted in the previous section.

3.5. Thermodynamic Stability. Finally we consider the relative stabilities of the UO_3 polymorphs under investigation with respect to pressure and present them in Figure 10.

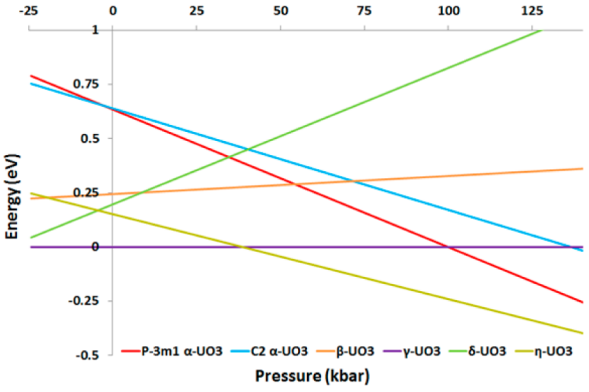

Figure 10. Calculated enthalpy of formation (ΔH_f) for UO_3 phases with PBE + U as a function of pressure, results are relative to γ-UO_3 (the thermodynamically most stable phase).

The enthalpy of formation for a UO_3 formula unit for each modification was calculated using the PBE + U computed UO_3, uranium metal, and O_2 free energies. The predicted energy of a U atom was found to be −8.43 eV, calculated from α-uranium using the parameters described in Section 2.1 but with a denser k-mesh of 175 k-points (12 × 8 × 8). The energy of an O atom was predicted to be −4.93 eV, calculated from an O_2 molecule in a 20 Å box using the Γ-point. Pressure has then been varied from −25 to 125 kbar (Figure 10) to provide a wide range of enthalpy values and simulate a range of conditions from high temperature (negative pressure) to high pressure (approaching 125 kbar). The stabilities in Figure 10 are presented relative to γ-UO_3, the thermodynamically most stable UO_3 polymorph from experiment,[64] and our PBE + U calculations.

At zero pressure the results show the PBE + U calculated order of stability as $H = U$. Here we can see that γ-UO_3 is the most stable polymorph and α-UO_3 is the least stable, in accordance with experimental measurements.[35] The γ-UO_3 polymorph is predicted to remain the most stable up to 39.5 kbar, at which point η-UO_3 becomes most stable. η-UO_3 is the densest polymorph (8.86 g cm^{-3}); described as high-pressure UO_3 it was first synthesized at 30 kbar and 1100 °C. Our calculations slightly overestimate this value but provide a good qualitative fit to the experimental data.[30] The $C2$ α-UO_3 structure is predicted to be more stable than its $P\bar{3}m1$ counterpart over the negative pressures (high temperatures) examined here but less stable at positive pressures with a widening stability gap. The large decrease in relative stability of δ-UO_3 with increasing pressure is most likely due to the considerably lower density of this polymorph (6.57 g cm^{-3}) compared to the others. Stability seems to be less related to the presence of uranyl bonding than the other properties that we have examined here, with no clear trend emerging.

4. CONCLUSIONS

PBE + U calculations of the UO_3 polymorphs were successfully applied to predict structural, elastic, and electronic properties, as well as assess their relative thermodynamic stability. We established that dispersive interactions are negligible using van der Waals corrected DFT and so only used DFT + U. We have demonstrated that the methodology is robust, simulating the full range of UO_3 structures. The best results are achieved for α- and δ-UO_3, which gives us confidence in modeling these U^{6+} phases. Those structures (β-, γ-, and η-UO_3) where we see larger differences we infer is due to a greater degree of nonstoichiometry. Indeed these structures contain a greater variety of U−O distances and U ions in very different coordination environments, which we believe is further evidence for the presence of defects.

We found imaginary modes for the experimentally reported $C2mm$ α-UO_3 structure, which were removed by applying small atomic displacements that lowered the symmetry to a $C2$ structure more closely resembling the $P\bar{3}m1$ polymorph. This leads us to conclude the $C2mm$ polymorph is a thermally averaged structure, and the $P\bar{3}m1$ structure is more representative of the actual material. Of the three γ-UO_3 polymorphs that were examined the monoclinic modification was found to relax to the $I4_1$ tetragonal cell, eliminating it as a viable structure. The $I4_1$ and $Fddd$ polymorphs are nearly identical, differing mainly in symmetry as the predicted energies and bond lengths are almost the same. As the two structures were recorded at different temperatures and the DFT calculations are performed at 0 K it follows that it is not straightforward to differentiate them using this methodology.

We have made predictions of the elastic constants and bulk moduli of the UO_3 polymorphs for the first time, finding them to generally have a lower bulk modulus than the denser-structured fluorite UO_2. The bulk modulus appears to be linked to the presence of uranyl bonds as well as the density. Oxides that contain uranyl bonds (β-, γ-, and η-UO_3) have lower bulk

dx.doi.org/10.1021/ic500791m | Inorg. Chem. 2014, 53, 12253−12264

moduli (<100 GPa), and those without uranyl bonds (α- and δ-UO_3) have higher bulk moduli (>150 GPa).

Our calculations generally reproduce experimentally determined band gaps well and reveal UO_3 to be a charge-transfer insulator. Small contributions from U 5f states to the O 2p-dominated VB and vice versa indicate a degree of covalency in the U−O bonding. The limited contributions from U 6d orbitals to the lower VB show the majority of bonding occurs through the 5f orbitals.

In accordance with experiment, we found γ-UO_3 to be the most thermodynamically stable, α-UO_3 the least stable, and η-UO_3 to be the high-pressure polymorph. The lowest-density polymorph δ-UO_3 is predicted to destabilize considerably with increasing pressure.

■ ASSOCIATED CONTENT

Ⓢ Supporting Information

PBE + U predicted structures for each polymorph, including lattice parameters and atomic coordinates, are provided (Tables S1−S8). Properties for each polymorph calculated with the pure PBE functional are also given (Tables S9−S11). Neutron diffraction patterns, RDFs, and PBE-computed DOS diagrams can also be found here. This material is available free of charge via the Internet at http://pubs.acs.org.

■ AUTHOR INFORMATION

Corresponding Author

*E-mail: s.c.parker@bath.ac.uk.

Notes

The authors declare no competing financial interest.

■ ACKNOWLEDGMENTS

Via our membership of the U.K. HPC Materials Chemistry Consortium, which is funded by EPSRC (EP/F067496 and EP/L000202), this work made use of the facilities of HECToR and ARCHER, the U.K. national high-performance computing service, which is provided by UoE HPCx Ltd. at the University of Edinburgh, Cray Inc., and NAG Ltd., and funded by the Office of Science and Technology through EPSRC High End Computing Programme. The authors would also like to acknowledge the University of Bath for the use of their HPC resources (Aquila). The authors would also like to acknowledge AWE for providing funding to conduct this research as well as the EPSRC (EP/I03601X/1).

■ REFERENCES

(1) Alberman, K. B.; Anderson, J. S. *Angew. Chem.* **1949**, *61*, 416−416.
(2) Hoekstra, H. R.; Siegel, S.; Fuchs, L. H.; Katz, J. J. *J. Phys. Chem.* **1955**, *59*, 136−138.
(3) Hoekstra, H. R.; Siegel, S. *J. Inorg. Nucl. Chem.* **1961**, *18*, 154−165.
(4) Hoekstra, H. R.; Siegel, S.; Gallaghe, F. *J. Inorg. Nucl. Chem.* **1970**, *32*, 3237−3248.
(5) Allen, G. C.; Crofts, J. A.; Curtis, M. T.; Tucker, P. M.; Chadwick, D.; Hampson, P. J. *J. Chem. Soc., Dalton Trans.* **1974**, *12*, 1296−1301.
(6) Allen, G. C.; Crofts, J. A.; Griffiths, A. J. *J. Nucl. Mater.* **1976**, *62*, 273−281.
(7) Allen, G. C.; Tempest, P. A.; Garner, C. D.; Ross, I.; Jones, D. J. *J. Phys. Chem.* **1985**, *89*, 1334−1336.
(8) Allen, G. C.; Holmes, N. R. *Appl. Spec.* **1994**, *48*, 525−530.
(9) Rousseau, G.; Desgranges, L.; Charlot, F.; Millot, N.; Niepce, J. C.; Pijolat, M.; Valdivieso, F.; Baldinozzi, G.; Berar, J. F. *J. Nucl. Mater.* **2006**, *355*, 10−20.
(10) Idriss, H. *Surf. Sci. Rep.* **2010**, *65*, 67−109.
(11) Faber, J.; Lander, G. H. *Phys. Rev. B* **1976**, *14*, 1151−1164.
(12) Fritz, I. J. *J. Appl. Phys.* **1976**, *47*, 4353−4358.
(13) Killeen, J. C. *J. Nucl. Mater.* **1980**, *88*, 185−192.
(14) Caciuffo, R.; Amoretti, G.; Santini, P.; Lander, G. H.; Kulda, J.; Du Plessis, P. D. *Phys. Rev. B* **1999**, *59*, 13892−13900.
(15) Desgranges, L.; Baldinozzi, G.; Rousseau, G.; Niepce, J.-C.; Calvarin, G. *Inorg. Chem.* **2009**, *48*, 7585−7592.
(16) Crocombette, J. P.; Jollet, F.; Nga, L. N.; Petit, T. *Phys. Rev. B* **2001**, *64*, 104107−104119.
(17) Laskowski, R.; Madsen, G. K. H.; Blaha, P.; Schwarz, K. *Phys. Rev. B* **2004**, *69*, 140480−140484.
(18) Freyss, M.; Petit, T.; Crocombette, J. P. *J. Nucl. Mater.* **2005**, *347*, 44−51.
(19) Geng, H. Y.; Chen, Y.; Kaneta, Y.; Iwasawa, M.; Ohnuma, T.; Kinoshita, M. *Phys. Rev. B* **2008**, *77*, 104120−104136.
(20) Dorado, B.; Amadon, B.; Freyss, M.; Bertolus, M. *Phys. Rev. B* **2009**, *79*, 235135−235143.
(21) Dorado, B.; Freyss, M.; Amadon, B.; Bertolus, M.; Jomard, G.; Garcia, P. *J. Phys.: Condens. Matter* **2013**, *25*, 33201−33201.
(22) Dorado, B.; Garcia, P. *Phys. Rev. B* **2013**, *87*, 195139−195146.
(23) McEachern, R. J.; Taylor, P. *J. Nucl. Mater.* **1998**, *254*, 87−121.
(24) Allen, G. C.; Holmes, N. R. *J. Nucl. Mater.* **1995**, *223*, 231−237.
(25) Allen, G. C.; Tempest, P. A. *J. Chem. Soc., Dalton Trans.* **1983**, *12*, 2673−2677.
(26) Andersson, D. A.; Espinosa-Faller, F. J.; Uberuaga, B. P.; Conradson, S. D. *J. Chem. Phys.* **2012**, *136*, 234702−234712.
(27) Andersson, D. A.; Baldinozzi, G.; Desgranges, L.; Conradson, D. R.; Conradson, S. D. *Inorg. Chem.* **2013**, *52*, 2769−2778.
(28) Benedict, M.; Pigford, T. H.; Levi, H. W. *Nuclear Chemical Engineering,* 2nd ed.; McGraw-Hill: New York, 1981.
(29) Sweet, L. E.; Blake, T. A.; Henager, C. H.; Hu, S. Y.; Johnson, T. J.; Meier, D. E.; Peper, S. M.; Schwantes, J. M. *J. Radioanal. Nucl. Chem.* **2013**, *296*, 105−110.
(30) Siegel, S.; Hoekstra, H.; Sherry, E. *Acta Crystallogr.* **1966**, *20*, 292−295.
(31) Cornman, W. R. *Preparation and Characterization of the Polymorphs of UO3;* United States Atomic Energy Comission, Savannah River Laboratory: Aiken, SC, 1962.
(32) Girgis, B. S.; Rofail, N. H. *J. Nucl. Mater.* **1992**, *195*, 126−133.
(33) Kovba, L. M.; Vidavskii, L. M.; Lavut, E. G. *Zh. Strukt. Khim.* **1963**, *4*, 627−629.
(34) Johnson, J. A. *Studies of Reaction Processes for Voloxidation Methods;* University of Tennessee: Knoxville, TN, 2013.
(35) Guillaumont, R.; Fanghänel, T.; Fuger, J.; Grenthe, I.; Neck, V.; Palmer, D. A.; Rand, M. H. *Update on the Chemical Thermodynamics of Uranium, Neptunium, Plutonium, Americium and Technetium;* Nuclear Energy Agency, Organisation for Economic Co-operation and Development: Amsterdam, 2003.
(36) Bagus, P. S.; Nelin, C. J.; Ilton, E. S. *J. Chem. Phys.* **2013**, *139*, 244704−244717.
(37) Bagus, P. S.; Ilton, E. S. *Top. Catal.* **2013**, *56*, 1121−1128.
(38) He, H. M.; Andersson, D. A.; Allred, D. D.; Rector, K. D. *J. Phys. Chem. C* **2013**, *117*, 16540−16551.
(39) Geng, H. Y.; Song, H. X.; Jin, K.; Xiang, S. K.; Wu, Q. *Phys. Rev. B* **2011**, *84*, 174115−174127.
(40) Pickard, C. J.; Winkler, B.; Chen, R. K.; Payne, M. C.; Lee, M. H.; Lin, J. S.; White, J. A.; Milman, V.; Vanderbilt, D. *Phys. Rev. Lett.* **2000**, *85*, 5122−5125.
(41) Kresse, G.; Furthmuller, J. *Comput. Mater. Sci.* **1996**, *6*, 15−50.
(42) Perdew, J. P.; Burke, K.; Ernzerhof, M. *Phys. Rev. Lett.* **1996**, *77*, 3865−3868.
(43) Castell, M. R.; Dudarev, S. L.; Muggelberg, C.; Sutton, A. P.; Briggs, G. A. D.; Goddard, D. T. *J. Vac. Sci. Technol., A* **1998**, *16*, 1055−1058.
(44) Yamazaki, T.; Kotani, A. *J. Phys. Soc. Jpn.* **1991**, *60*, 49−52.
(45) Nerikar, P.; Watanabe, T.; Tulenko, J. S.; Phillpot, S. R.; Sinnott, S. B. *J. Nucl. Mater.* **2009**, *384*, 61−69.

(46) Dorado, B.; Garcia, P.; Carlot, G.; Davoisne, C.; Fraczkiewicz, M.; Pasquet, B.; Freyss, M.; Valot, C.; Baldinozzi, G.; Simeone, D.; Bertolus, M. *Phys. Rev. B* **2011**, *83*, 035126−035136.
(47) Dorado, B.; Andersson, D. A.; Stanek, C. R.; Bertolus, M.; Uberuaga, B. P.; Martin, G.; Freyss, M.; Garcia, P. *Phys. Rev. B* **2012**, *86*, 035110−035120.
(48) Dorado, B.; Garcia, P. *Phys. Rev. B* **2013**, *87*, 195139−195146.
(49) Momma, K.; Izumi, F. *J. Appl. Crystallogr.* **2011**, *44*, 1272−1276.
(50) Le Page, Y.; Saxe, P. *Phys. Rev. B* **2002**, *65*, 104104−104118.
(51) Ravindran, P.; Fast, L.; Korzhavyi, P. A.; Johansson, B.; Wills, J.; Eriksson, O. *J. Appl. Phys.* **1998**, *84* (9), 4891−4904.
(52) Fast, L.; Wills, J. M.; Johansson, B.; Eriksson, O. *Phys. Rev. B* **1995**, *51*, 17431−17438.
(53) Hebbache, M.; Zemzemi, M. *Phys. Rev. B* **2004**, *70*, 224107−224113.
(54) *Materials Studio,* 5.5.0.0; Accelrys Software Inc.: San Diego, CA, 2013.
(55) Zachariasen, W. H. *Acta Crystallogr.* **1948**, *1*, 265−269.
(56) Loopstra, B. O.; Cordfunk, E. H. P. *Recl. Trav. Chim. Pays-Bas* **1966**, *85*, 135−142.
(57) Debets, P. C. *Acta Crystallogr.* **1966**, *21*, 589−593.
(58) Loopstra, B. O.; Taylor, J. C.; Waugh, A. B. *J. Solid. State Chem.* **1977**, *20*, 9−19.
(59) Weller, M. T.; Dickens, P. G.; Penny, D. J. *Polymer* **1988**, *7*, 243−244.
(60) Kim, B. H.; Lee, Y. B.; Prelas, M. A.; Ghosh, T. K. *J. Rad. Nucl. Chem.* **2012**, *292*, 1075−1083.
(61) Greaves, C.; Fender, B. E. F. *Acta Crystallogr., Sect. B: Struct. Sci.* **1972**, *28*, 3609−3614.
(62) Debets, P. C. *J. Inorg. Nucl. Chemistry* **1964**, *26*, 1468−1470.
(63) Cordfunke, E. H. P.; Westrum, E. F. *Thermochim. Acta* **1988**, *124*, 285−296.
(64) Cordfunke, E. H.; Aling, P. *Trans. Faraday Soc.* **1965**, *61*, 50−53.
(65) Engmann, R.; Wolff, P. M. D. *Acta Crystallogr.* **1963**, *16*, 993−996.
(66) Grimme, S.; Antony, J.; Ehrlich, S.; Krieg, S. *J. Chem. Phys.* **2010**, *132*, 154104−150123.
(67) Ding, H.; Xu, B. *J. Chem. Phys.* **2012**, *137*, 224509−224515.
(68) Londero, E.; Schröder, E. *Phys. Rev. B* **2010**, *82*, 054116−054124.
(69) Wheeler, V. J.; Dell, R. M.; Wait, E. *J. Inorg. Nucl. Chem.* **1964**, *26*, 1829−1845.
(70) *Powder Cell,* 2.3; BAM: Berlin, Germany, 2014.